Experimental Study on Strong Interaction between Regular Waves and Wind Waves-?

Tôhoku Geophys. Journ., (Sci. Rep. Tôhoku Univ., Ser. 5), Vol. 28, No. 2, pp. 87–103, 1981.

Experimental Study on Strong Interaction Between Regular Waves and Wind Waves–II

YUTAKA IMAI*, MITSUHIKO HATORI, MASAYUKI TOKUDA**
and YOSHIAKI TOBA

Geophysical Institute, Faculty of Science, Tohoku University
Sendai 980, Japan

(Received June 16, 1981)

Abstract: Experiments on evolution of a wave field, when the wind blows over a train of mechanically generated regular wave, have been performed in a wind-wave tunnel. Among four stages of the evolution already described in the preceding paper (Hatori *et al.*, 1981), the passage from the first to the second stages, where attenuation of local wind waves and simultaneous growth of regular waves begin to take place, has been investigated in detail. Statistical investigation using individual-wave analysis technique is made. Analyses using the phase (location of wind wave crest on regular wave)-frequency (of wind wave) diagram show a clear systematic tendency suggesting the existence of nonlinear interactions between wind wave component and regular wave component in the second stage. Case studies of tracing evolution of local wind waves with respect to the phase of co-existing regular wave suggest that the strong interaction occurs among the regular wave and one or two crests of local wind waves located near the crest of the regular wave.

1. Introduction

In the preceding paper (Hatori *et al.*, 1981, hereafter referred to as I), the evolution of wave fields under the co-existence of mechanically generated regular waves and the wind waves was studied by use of a wind-wave tank of 20 m in length. Investigation based on spectral analysis of wave records revealed that the evolution of such wave field was divided into the following four stages: Stage 1 where the regular wave component did not develop substantially and the wind wave component grew independently; Stage 2 where the regular wave component began to grow rapidly and at the same time the growth of wind wave component diminished remarkably in comparison to the case of pure wind waves; Stage 3 where the spectral peak of the wind wave component disappeared and only the regular wave component grew; and Stage 4 where the regular wave component attained a random nature similar to that of the wind waves. From this the existence of some strongly nonlinear interactions was suggested in the co-existing system of regular wave and local wind waves.

Many experiments using mechanically-generated regular waves have been performed in recent years to verify the Miles' (1960) mechanism of wind wave generation (e.g., Bole and Hsu, 1969 and Mizuno, 1975). However, experimental results of I

* Present address: Kokusai Kogyo Co., Ltd., Hino Technical Division, Hino 191, Japan
** Present address: Institute of Coastal Oceanograpy, National Research Center for Disaster Prevention, Hiratsuka 256, Japan

demonstrated evidently the inapplicability of such experiments using regular waves for the verification of the theory. The results seem to show that the situation where wind blows over regular waves should be rather regarded as a model of sea field where swells and wind waves co-exist. Further, the existence of the strong interaction at Stage 2 presents a doubt whether the evolution of swell-sea field can be properly explained by the theories of weakly nonlinear interactions of component waves as proposed by Hasselmann (1962, 1963). In fact, there are recent studies showing that strongly nonlinear characteristics must be important in the evolution of wave field as reviewed by Yuen and Lake (1980).

The main purpose of the present study is to investigate closely the mechanism of strong interaction noticed especially in Stage 2. For this purpose a smaller wind wave tank has been used, and a new way of approach by use of individual wave analyses is introduced.

The individual waves were defined as the actual undulations of the water surface at any instant by Toba (1978) and Tokuda and Toba (1981), and regarded as characterized by concentrated shearing stress and a strong vortical region at their crests as studied by Toba *et al.* (1975), Okuda *et al.* (1977) and Okuda (1981). The individual-wave method is expected to be useful for the present case of the co-existence of regular wave and wind wave, especially for the study of evolution of local wind waves with respect to the phase, or relative location, of the regular wave.

2. Experiment and analysis of data

2.1. Equipment and procedure of experiment

The experiments were made in a wind-wave tunnel of 850 cm in length, 15 cm in width and 70 cm in height, containing 48 cm deep water, as shown in Fig. 1. A blower is installed in the upstream extension, a plunger-type wave generator at the upstream end of the tank, and a permeable wave absorber at the downstream end. The wind is introduced on the water surface free from the influence of the plunger through a

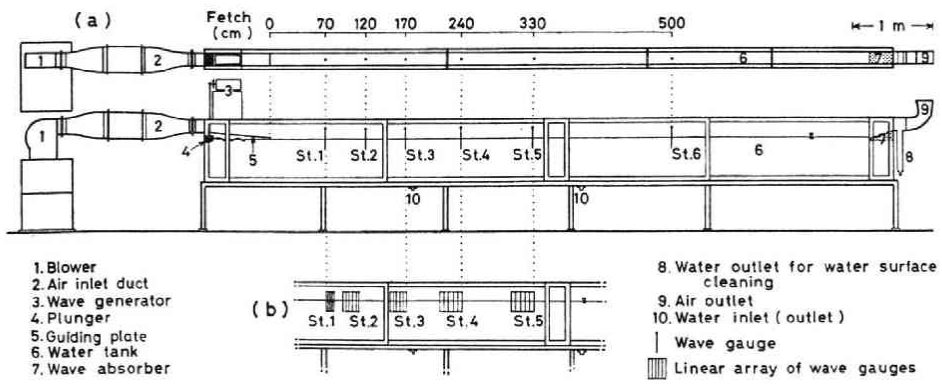

Fig. 1. A schematic view of the wind-wave tunnel, and measurement stations (a) for the simultaneous wave measurements and (b) for the measurements using the linear array of wave gauges.

Table 1. Fetch of stations for simultaneous wave measurements.

Station No.	1	2*	3	4*	5	6
Fetch (m)	0.7	1.2	1.7	2.4	3.3	5.5

* Stations where wind profile was also measured.

Table 2. Abbreviation of experimental conditions.

Friction velocity u_* (m s^{-1})	0	0.40	0.54	0.69
With regular wave	R	RU1	RU2*	RU3
Without regular wave	—	U1	U2	U3

* Wave measurements using the linear array of wave gauges were performed.

guiding plate of a slope of 8/100, at 81 cm from the upstream end of the tank. The distance from the end of the plate to this still water surface is fixed to 2.3 cm.

Water surface displacements were measured with capacitance-type wave gauges simultaneously at 6 stations, from Station 1 to Station 6, indicated in Fig. 1 (a) and in Table 1. The measurements were performed for each case shown in Table 2. Only one kind of regular wave of period T=0.44 s and wave height H=0.40 cm (steepness δ=0.01) was used. We used three ranges of wind speeds, and for each range we measured wind speed profiles with a pitot-static tube at Stations 2 and 4, and from these profiles an averaged friction velocity was obtained as shown in Table 2. For each wind condition we measured the waves for two conditions, that is, with and without the regular wave. The wave measurements were also made for the case of no wind on the regular wave. The conditions of the regular wave and of the winds were so selected that Stages 1 and 2 could be realized.

Table 3. Fetch of stations and intervals of neighbouring wave gauges, for a linear array of six wave gauges in Case RU2.

Station No.	1	2	3	4	5
Fetch of most upstream gauge (m)	0.7	0.9	1.5	2.1	3.0
Interval of wave gauges (cm)	2.0	4.0	4.0	6.0	6.0

In addition to the above wave measurements, we performed a different type of measurement for the case RU2, by use of a linear array of six wave gauges arranged in a line along the fetch direction as shown in (b) of Fig. 1 and in Table 3. This special measurement was performed with the aim of tracing the deformation of individual waves closely as described later.

2.2. *Analysis of the wave data*

Wave records of each run were digitized at a sampling frequency of 50 Hz. Each of the wave data was divided into five sub-samples of 40.96 s, which contained 2048 data points.

The time series data of the cases RU1, RU2 and RU3, in which regular waves and wind waves co-exist, was separated into two component time series of regular wave and wind wave, by use of a special procedure of numerical filtering, which is schematically shown in Fig. 2, and which is composed of the following four processes. (i) The wind wave components are cut off from the raw data by taking a moving weighted average of

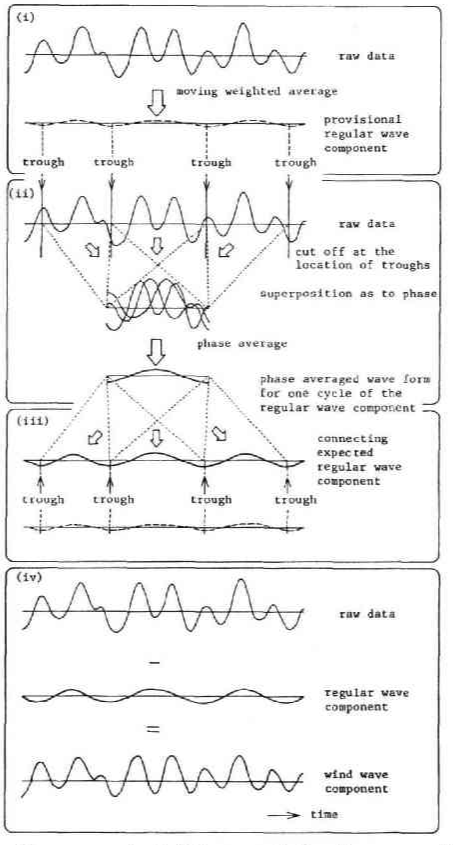

Fig. 2. A procedure for the numerical filter used for the separation of the regular wave component and the wind wave component. See the text.

the raw time series data, which corresponds to the low pass filter having a cut off frequency of 3.5 Hz. The regular wave component obtained by this process is not satisfactory since its higher harmonics are lost. We use this process only to determine the location of troughs of individual regular waves. (ii) The raw data is cut off at the location of troughs determined by item (i), and all divisions are superposed. In the superposition, the phase with respect to the length of a division is adopted as the phase of the respective regular wave, since the period of regular waves has some slight fluctuation owing to the modulation. Thus the phase averaged wave form for one cycle of the regular wave component can be obtained. (iii) The time series data of regular wave component is synthesized by connecting, in turn, the average regular wave

form, which is expanded or contracted in its time axis according to the fluctuation of period, at the location of regular wave troughs determined by (i). (iv) By subtracting this time series of regular wave component from the raw data, the component time series of wind wave is yielded.

This tedious filtering procedure has the following merits. First, disregard of the fluctuation of regular wave periods by modulation is avoided in the process of the phase averaging. Second, higher harmonics of regular wave component are retained in the time series of regular wave component, without contaminating wind wave component.

The time series data of the two components are further analysed by use of the individual-wave method, the details of which are given by Tokuda and Toba (1981). Each time series data is divided into individual waves according to zero-crossing trough-to-trough (ZCTT) scheme. These individual waves are classified into frequency bands having the same band width Δf of 1/5.12 Hz, according to their frequency f defined as the reciprocal of its period T.

For each frequency band, designated by the subscript i and having the center frequency f_i, we obtain the mean period T_i, mean wave height H_i and number m_i of individual waves contained in each frequency band. The energy density ϕ_i is defined in accordance with Tokuda and Toba (1981) as,

$$\phi_i = \frac{m_i T_i H_i^2}{8 \Delta f \sum_i m_i T_i}, \tag{1}$$

where the sum is taken for all frequency bands i.

Similarly the number density per unit time and unit frequency M_i is given by

$$M_i = \frac{m_i}{\Delta f \sum m_i T_i}. \tag{2}$$

Thus we have obtained the frequency (or period) distributions of mean wave height, number density and energy density (i.e. power spectra) for individual waves.

For the purpose of comparison we have also calculated the power spectra by the FFT method under absolutely the same resolution band width as used in the individual wave method. Spectra obtained by the above two ways for each wind wave component and regular wave component have almost agreed with each other in the main frequency range, just as shown by Tokuda and Toba (1981) for spectra of wind waves.

Further, we have arranged the individual waves of wind wave component into eight phase bands with respect to regular wave component in addition to the frequency classification. Here, the phase of each individual wave of wind wave component with respect to regular wave component denotes the relative location of its crest to that of the regular wave. The phase is defined 0° at the crest of regular wave, 180° at the trough on the downwind and −180° at that on the upwind side, and the range from −180° to 180° is divided into eight bands each having the width $\Delta\theta$ of 45°.

For this case of phase-frequency classification, we have reset the frequency band width of 1/2.56 Hz to compensate the reduction of number of individual waves contained within each phase-frequency mesh. The energy density ϕ_{ij} per unit frequency and unit phase of the regular wave is given by

$$\phi_{ij} = \frac{m_{ij} T_{ij} H_{ij}^2}{8 \Delta f \sum_i \sum_j m_{ij} T_{ij}} \cdot \frac{360^\circ}{\Delta\theta}, \tag{3}$$

and the number density per unit time, unit frequency and unit phase of the regular wave by

$$M_{ij} = \frac{m_{ij}}{\Delta f \sum_i \sum_j m_{ij} T_{ij}} \cdot \frac{360^\circ}{\Delta\theta}, \tag{4}$$

where the phase is measured by the degree and is normalized by 360°. In the above two equations (3) and (4), H_{ij}, T_{ij} and m_{ij} are, respectively, the mean wave height, the mean period and the number of individual waves for each mesh designated by ij, and the summations in the denominator are taken for all frequency and phase bands i and j, respectively.

Finally, based on the data for the case RU2 obtained by using the linear array, we have traced the evolutions of wave heights and energy densities of individual wind wave crests on a frequency (of wind wave)-phase (of regular wave) plane. A detailed description of the data processing is as follows. Since the interval of neighbouring wave gauges of the array listed in Table 3 is selected to be of the same order as the main wave length of wind waves, each individual wave can be traced on the set of six time series data. The difference of the values of wave height or period of each individual wave between the first and the sixth wave gauges is significant. For the identification of the location of a wind wave crest on the frequency-phase plane, the mean values of the first and sixth data were used. The mean wave height and the energy density are then calculated for both the first and the sixth wave gauge data series, for each frequency-phase mesh. Subtracting the values for the first data from those for the sixth data, we can obtain the frequency-phase distributions of evolutions of wave height and energy density.

3. Experimental results

3.1. Statistical properties of co-existing wave field in comparison with pure wind wave case

First a comparison is made of the frequency (or period) distributions of energy density, mean wave height and number density in cases where the regular waves and the wind waves co-existed, with the corresponding values of the pure wind wave cases. The power spectra obtained by the individual wave method for the six stations for the case RU2 are shown in Fig. 3 (thick lines) along with the spectra for the pure wind wave case of the same wind speed, U2 (thin lines). For the other two cases RU1 and RU3,

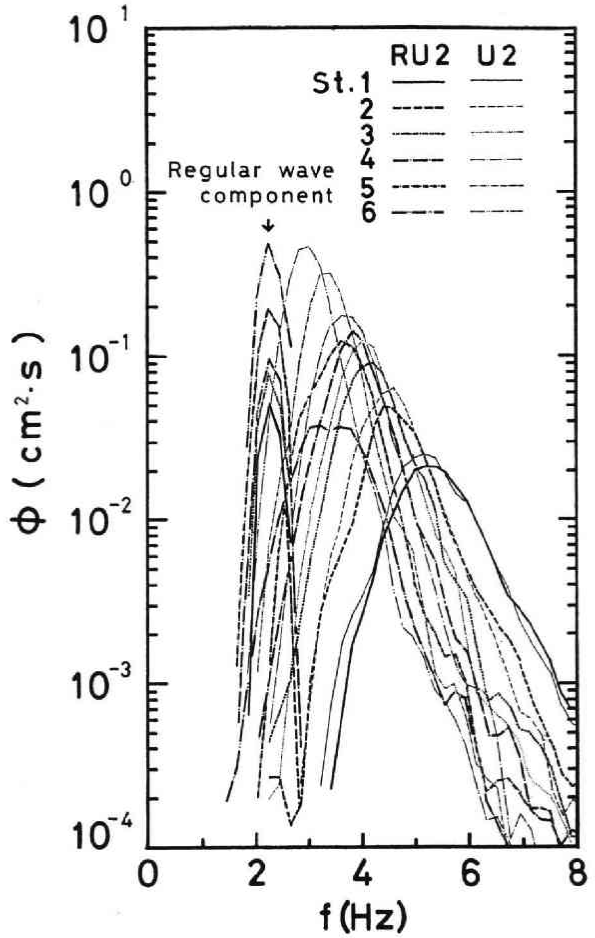

Fig. 3. A comparison of the evolution with fetch of energy spectrum ϕ for the case RU2 (thick lines) with that for the pure wind wave case U2 (thin lines).

similar results are obtained as the case RU2. Consequently the case RU2 will be treated as a representative one.

The evolution of the power spectra in the fetch direction is substantially similar to that shown in I, and we can clearly say that we have achieved the Stages 1 and 2 of evolution. Namely, at Stations 1 and 2, corresponding to the first stage, the regular wave component indicated by the arrow does not grow and only the wind wave component grows in exactly the same way as the pure wind wave case. From Stations 3 to 6, corresponding to Stages 2, the regular wave component grows rapidly, while the growth of the wind wave component diminishes in comparison to the pure wind wave case, and at Station 6 the energy of wind wave component is very small. In Stage 2 it is noticed that the reduction of energy density of the wind wave component in comparison to the pure wind wave case occurs mainly in the frequencies ranging from the dominant energy range to the lower frequency side. It should be noticed that the difference of

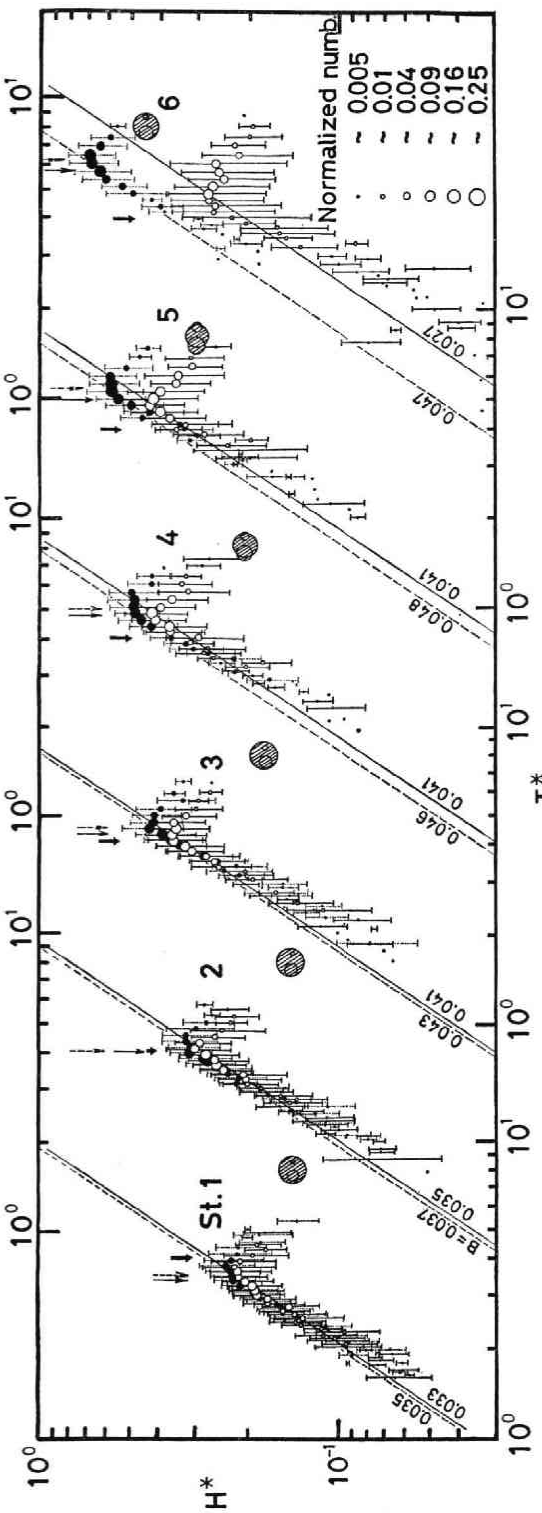

Fig. 4. Distributions of the nondimensional wave height H^* against the nondimensional period T^* for six fetches. Open and striped circles represent the wind wave component and the regular wave component of the case RU2 respectively, and solid circles represent the case U2. Solid and dashed arrows indicate the periods of spectral peak for the wind wave component of RU2 and for U2, respectively, and large solid arrows indicate the periods of the second harmonics of the regular wave component.

Fig. 3 from Figs. 2(b) and 3(b) in I lies in the point that in Fig. 3 there is no energy at the frequency of higher harmonics, the energy of forced waves being included in the primary frequency by use of the special filtering technique described in the last section. Another difference is seen in that there are two power spectral densities at the same frequency near the regular wave component. This is the consequence of the separation of wave records into the two component time series of wind wave and regular wave, by use of the filter described in *2.2*.

In Fig. 4, the nondimensional mean wave heights of individual waves $H^*(\equiv gH/U_*^2$, g: the acceleration of gravity) are plotted against the nondimensional period $T^*(\equiv gT/U_*)$. The open and striped circles represent the wind wave component and the regular wave component of the case RU2, respectively. The size of circles indicates the number density and the bar the standard deviation of H^* in each frequency band. The solid circles, representing the pure wind wave for the case U2, are distributed along the line of the 3/2-power law (Toba, 1972, 1978): $H^*=BT^{*3/2}$ for the higher frequency range in the same way as shown by Tokuda and Toba (1981) with the same value of the coefficient B.

The distributions of the case RU2 evolve with fetch as follows. At Stations 1 and 2, corresponding to Stage 1, distributions of the wind wave component almost agree with those of pure wind waves, and the mean wave height of regular waves does not

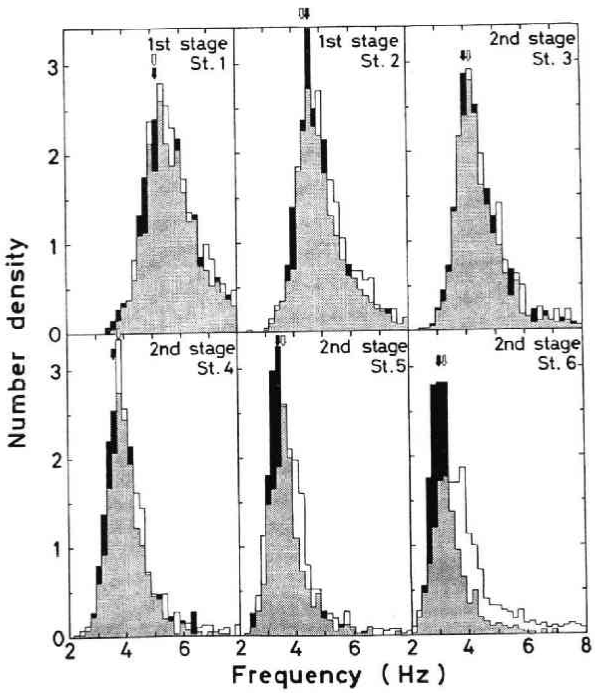

Fig. 5. Frequency distributions of the number density of individual waves of the wind wave component (RU2, open area) and of the pure wind waves (U2, filled up area). Screened area denote the overlapping portion. Arrows indicate the spectral peak frequency.

show appreciable change with the fetch. From Stations 3 to 6 (Stage 2), the mean wave heights of wind wave component decrease rapidly with the fetch in comparison with those of pure wind waves, mainly in the range of period higher (lower frequency) than that of the respective spectral peak. The mean wave heights in the lower periods also show a slight decrease, but they are still distributed almost along the line of 3/2 power but with lower values of B. Corresponding to this decrease of wind wave component, the wave heights of regular wave component (striped circles) increase very rapidly. The decrease in the energy density or wave height of wind wave component and the increase in that of regular wave component observed in Stage 2, clearly suggest the energy transfer to the regular wave component from the wind wave component.

Fig. 5 shows the frequency distributions of the number densities of individual waves of both the wind wave component (RU2, the open area) and the pure wind waves (U2, the filled up area) at each station. The screened area represents the overlapping. It is seen from this figure that at Stage 1 (Stations 1 and 2) the distribution for the wind wave component agrees with that for the corresponding pure wind wave case, and also that at Stage 2 (Stations 3, 4, 5 and 6) the number density of the wind wave

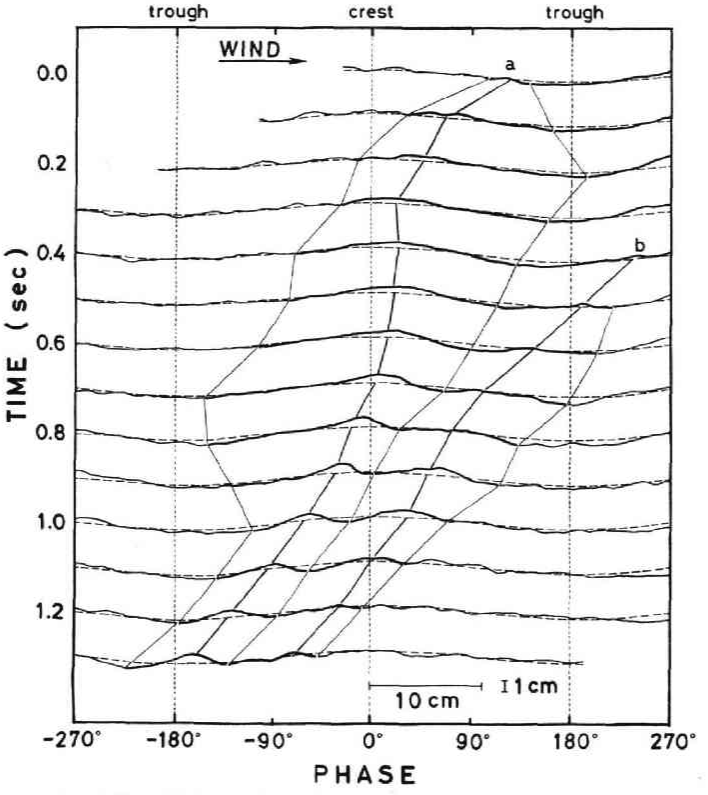

Fig. 6. An example of time history of spatial wave forms in a frame moving with the regular wave component (dashed lines) for the case RU2. Time increases downwards with an interval of 0.1 s and wind blows from left to right.

component decreases in the lower frequency range and on the other hand increases in the higher frequency range in comparison to the pure wind waves, and the trend becomes remarkable with the fetch.

Since the energy density of individual waves is related to the band averaged wave height and the number density by equations (1) and (2), the trends seen in Stage 2 of Figs. 3, 4 and 5 are related to each other as follows. Large decrease of both the wave height and the number density of the wind wave component in the frequency range lower than its spectral peak relative to that of the pure wind wave cases, corresponds to the energy density decrease. In the frequency range higher than the peak, the relatively slight decrease of wave height cancel out the excess of number density, to keep the energy density of the wind wave component as the same degree as that of the pure wind waves.

3.2. The frequency-phase distributions

The results described in *3.1*, obtained by the new technique of the individual-wave analysis, support the results in I, where it was shown that there was some strong interaction between regular waves and wind waves at Stage 2. Here, in order to clarify further the mechanism of the strong interaction, we examine the time-space variation of local wind waves with respect to phase of regular waves.

Fig. 6 shows a typical sequence of the surface profile relative to the regular wave, traced from a shadowgraph stroboscopic film taken from the side of the wind-wave tunnel, including Stations 5 and 6 within the sight. In Fig. 6, time increased downwards with an interval of 0.1 s. The individual waves of the wind wave component, having phase speeds smaller than that of the regular wave, travel from the right (down wind) to the left relative to the regular wave whose profile is shown by broken lines. As a wave named '*a*' proceeds to the crest of regular wave from the leeward side, its wave height, wave length and phase speed increase. When it reaches near the crest, it is trapped there and increases its wave height. Then, when another wind wave named '*b*' approaches from the lee side, '*a*' resumes its progress to the windward side and becomes smaller, and '*b*' becomes larger simultaneously, then '*b*' becomes small to give energy to the regular wave. Such a systematic change of local wind waves relative to the regular wave form as seen by this example is observed significantly often at fetches corresponding to Stage 2. Another case was also observed, where the wave '*a*' was not accompanied by the second wave '*b*', during similar passage of the interaction.

From the above facts, it is expected that the energy spectra, the frequency-band averaged wave height and the number density of individual wind wave crests vary according to their location relative to the regular wave form, that is, according to the phase of regular wave. As an enormous labor is needed to gain enough data of individual waves from this kind of spatial wave series on a film, we hereafter use the time series data.

Figs. 7(a), (b) and (c) show the frequency-phase distributions of the energy density ϕ_{ij}, the mesh-averaged wave height H_{ij} and the number density M_{ij} of wind wave

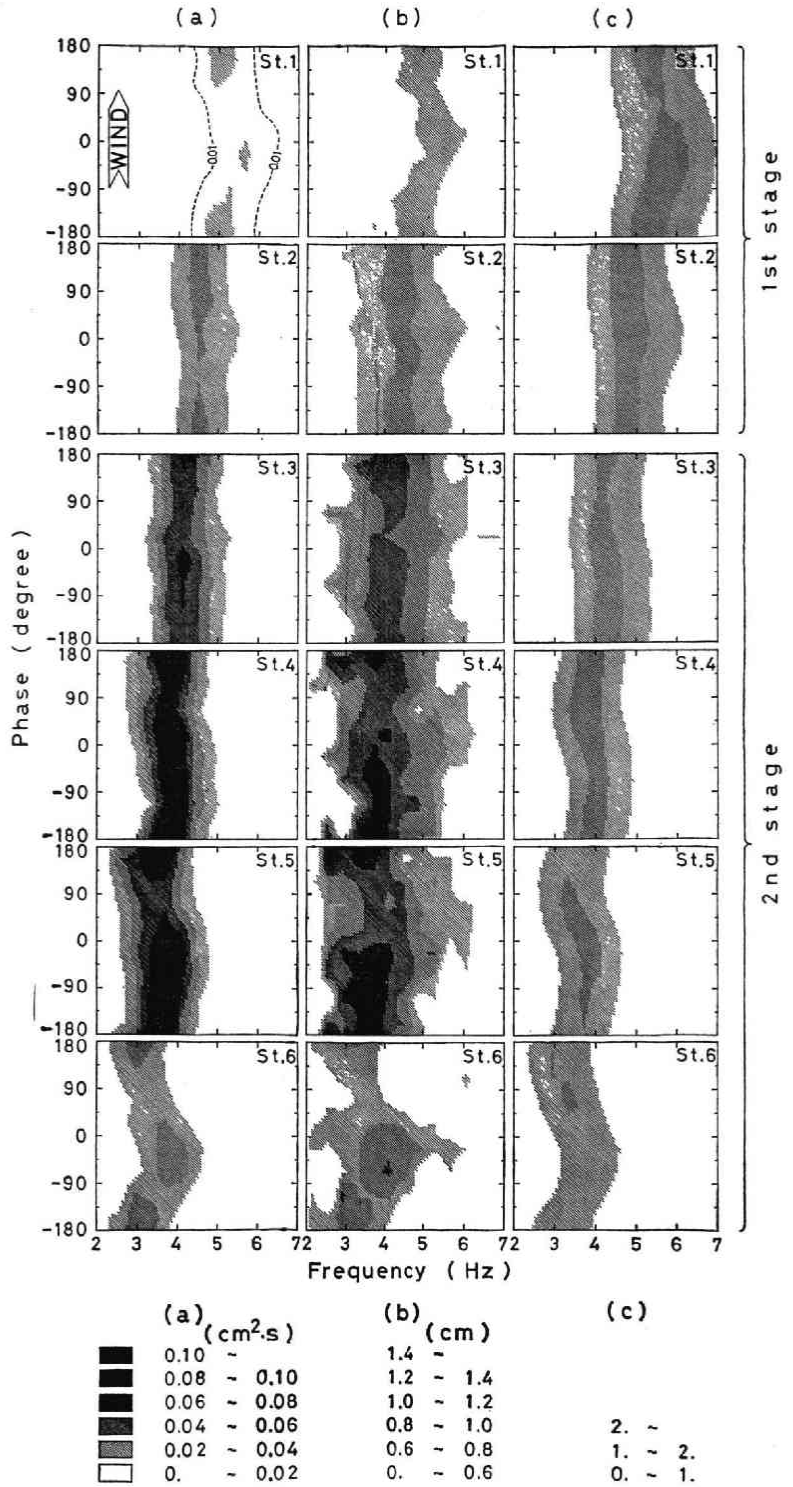

Fig. 7. Frequency (wind wave)-phase (regular wave) distributions of (a) energy density ϕ_{ij}, (b) wave height H_{ij} and (c) number density M_{ij}.

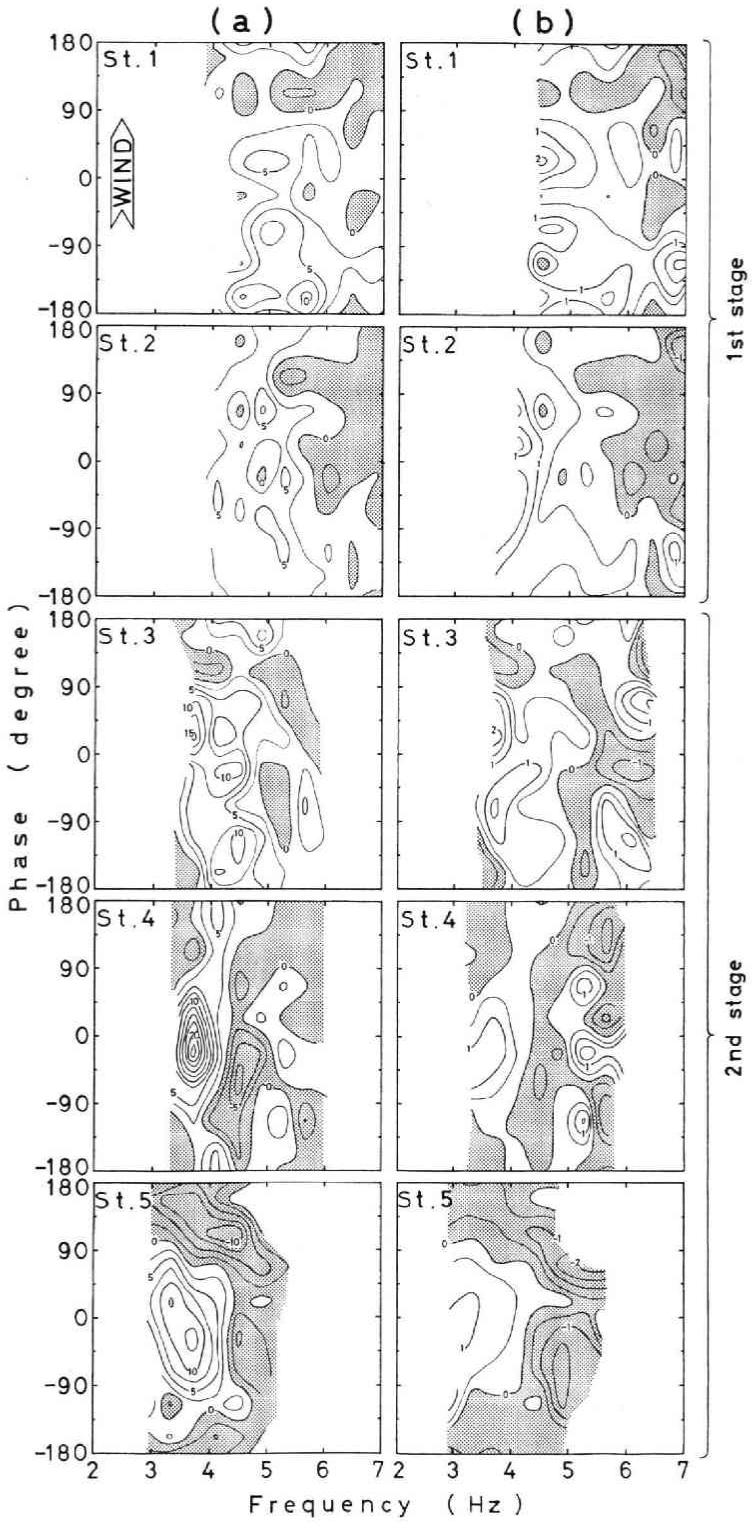

Fig. 8. Frequency-phase distributions of the variation per unit length (cm) in energy density ($\times 10^{-4}$ cm^2) (a) and in wave height ($\times 10^{-2}$ cm) (b).

component, respectively, at the six stations listed in Table 1. The average of Fig. 7(a), (b) or (c) through the entire phase gives Fig. 3, 4 or 5, respectively. From these distributions in Fig. 7 we can observe the following trends with phase.

Every distribution in Stage 1 (Stations 1 and 2) shows little variation with phase, except the slight inclination toward higher frequency near the crest (0°) of regular wave component at Station 1. In Stage 2 (Stations 3 to 6) the energy density and the averaged wave height are relatively high over the windward side down to the trough (about 0° to −180°) and low on the leeward side (about 45° to 90°), and this tendency becomes remarkable with fetch. The distributions of number density in this stage tend toward higher and lower frequencies in upwind and downwind sides of the crest, respectively, and this also becomes remarkable with the fetch.

Figs. 8(a) and (b), which were made for a more direct understanding of the process, show the frequency-phase distributions of the variation in energy density and wave height, respectively, for five stations listed in Table 3. It should be noted that the variation represents the mesh averaged evolution of individual waves obtained by tracing them as described in the last part of *2.2*. In this figure the shaded area corresponds to decreasing values and the other area to the increasing. The distinguished feature seen in Stage 2 (Stations 3 to 5) in both the (a) and (b), which is absent in Stage 1 (Stations 1 and 2), is the strong increase in the lower frequency side near the crest of regular wave, and the decrease in the higher frequency side on the upwind side of the crest.

This feature in Stage 2 seems to be consistent with the results already shown in other figures. We will discuss, in the succeeding section, the strong interaction further by relating all these results.

4. Discussion

It should be meaningful to discuss these figures taking into account the trajectories of individual waves. Although the trajectories of individual wave will scatter considerably, they seem to be traced, in an average, along a curve in Fig. 9, which is drawn on the figure at Station 4 in Fig. 8(a). The curve was drawn based on repeated observations of the process filmed by a 16-mm cinecamera whose typical trace was shown in Fig. 6.

Taking this trajectory into account, let us re-examine the results in Figs. 7 and 8. The local wind wave, in Fig. 8, having traveled along this trajectory from the leeward side to the region near the crest of the regular wave, enters the region of increasing wave height. The location of this increasing region seems to agree with the beginning of the region of higher energy density and higher wave height in Figs. 7(a) and (b).

After this the wave moves along the curve into region of decreasing, and becomes a small wave. The shift of the number density distribution toward higher frequencies on the windward side of regular wave crest may be explained as due to the formation of the smaller waves by these processes.

The results, together with those of I, indicate clearly that the wave field created

by wind-exerted regular waves is not so simple as that the regular wave grows by the wind action, free from the influence of other components. It should rather be considered that this kind of wave field is a model of the actual swell-sea field. Although Hasselmann (1963) treated theoretically the swell-sea interaction, it gives the swell

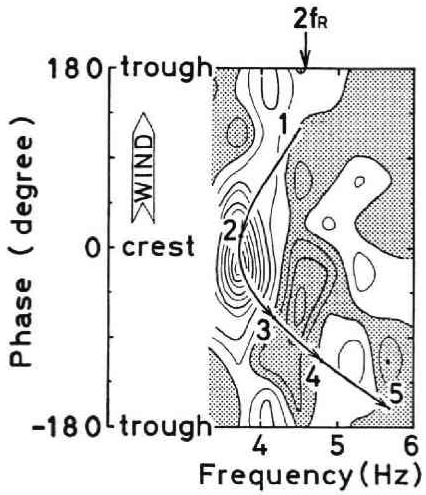

Fig. 9. A schematic mean locus of local wind waves on the phase-frequency plane superposed on the figure of Station 4 in Fig. 8(a).

attenuation and seems to contradict at least with the rapid growth of regular wave component in Stage 2. Clearly, this nonlinear theory gives no information about such a systematic distribution of wave energy in the frequency-phase plane as seen in Figs. 7 and 8.

A theoretical treatment of changes in the form of short gravity waves on long waves was also given by Longuet-Higgins and Stewart (1960). According to their theory, the energy transfer between short waves and long waves is conservative, and the wave height of short waves takes maximum and minimum values at just the crest and the trough of long waves, respectively, and the wave length changes in a converse way. On the contrary, the net energy transfer expected from our result at Stage 2 seems one-way from the wind wave component to the regular wave component.

Phillips and Banner (1974) have also proposed a theory on a similar case taking wind drift and wave breaking into consideration. The reduction of wind wave component in Stage 2 seems qualitatively consistent with their theory, but we have not observed wave breakings of the wind wave component around the regular wave crest in spite of their very large increase in wave heights around the crest. The disagreement between our result and these theories is considered to be caused by the difference in scales of short waves with respect to long waves: in our experiment the frequency of main wind wave component is about twice of that of regular wave component, in contrast to these theories.

We can suggest a schematic model for this strong interaction drawn from our

experimental results, as shown in Fig. 10. The wind wave '*a*' increases its wave height, wave length and phase speed in approaching the regular wave crest form its leeward face (1 in Fig. 10). When reaching close to the crest, it is exerted by the wind stress more strongly and increases the wave height and phase speed rapidly (2 in Fig. 10). The phase speed sometimes becomes large enough for this wave to be trapped on the

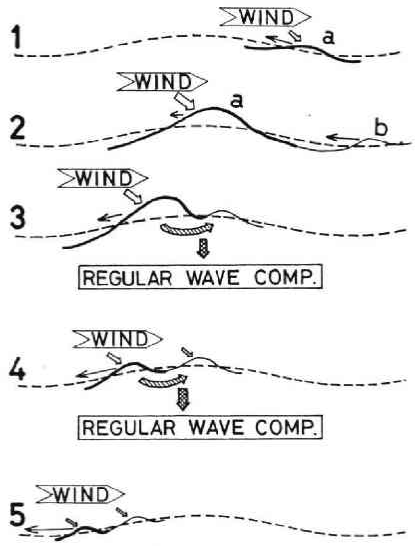

Fig. 10. Schematic representation of the strong interactions.

regular wave crest. The extension of its staying time at the crest allows its further growth by the wind, until the approach of a next wave '*b*' to the crest from the leeward side. This approach causes an energy transfer from '*a*' to '*b*', then to the regular wave (3 in Fig. 10). Then '*a*' and '*b*' depart the crest and the energy is transferred to the regular wave component. In this process it is speculated that the existence of a strong vortical layer near the wave crest, as studied by Okuda (1981), may be important (4 in Fig. 10). The secondary wind wave '*b*' seems to act as the mediator for this energy transfer. The departed wind waves '*a*' and '*b*' from the regular wave crest travels on its windward face and becomes smaller in wave height, wave length and phase speed (5 in Fig. 10). The above model was constructed from the frequently observed case of the evolution of the co-existent system, which is shown in Fig. 6. It should be noted, however, that another model, in which the wave '*b*' does not exist, may also be considerable. All of the experimental results obtained from the series of our study seem to indicate some strong interactions, which may not be explained by any existing theories, among the local wind wave, the regular wave and the wind, causing efficient energy transfer from the wind to the wave.

These new aspects of interactions seem to proceed when the frequency of wind wave component becomes close to that of the second harmonics of the regular wave. There is a possibility that the co-existence under the wind of longer wave and shorter

wave, of which the frequency is comparable to that of second harmonics of the longer wave, is a system which may effectively transfer energy from the wind to the longer wave, through some strongly nonlinear interactions including local wind drift. A further discussion relating to the inclusion of the second harmonics is given in Toba *et al.* (1981).

In ocean wave prediction problems, we frequently encounter situations with the co-existence of swells and wind waves. It should be essential for us to make a systematic study of these strong interactions for this purpose also.

Acknowledgments: Valuable discussion by Drs. S. Kawai, K. Okuda, M. Koga and assistance by Miss Yoko Inohana of the laboratory are very much appreciated. This study was partially supported by the Grant-in-Aid for Scientific Research by the Ministry of Education, Science and Culture, Project No. 374020.

References

Bole, J.B. and E.Y. Hsu, 1969: Response of gravity water waves to wind excitation. *J. Fluid Mech.*, **35**, 657–675.

Hasselmann, K., 1962, 1963: On the non-linear energy transfer in a gravity-wave spectrum. Part 1. General theory. *J. Fluid Mech.*, **12**, 481–500. Part 2. Conservation theorems. ibid., **15**, 273–281. Part 3. Evaluation of the energy flux and swell-sea interaction for a Neumann spectrum. ibid., **15**, 385–398.

Hatori, M., M. Tokuda and Y. Toba, 1981: Experimental study on strong interaction between regular waves and wind waves – I. *J. Oceanogr. Soc. Japan*, **37**, 111–119.

Longuet-Higgins, M.S. and R.W. Stewart, 1960: Changes in the form of short gravity waves on long waves and tidal currents. *J. Fluid Mech.*, **8**, 565–583.

Miles, J.W., 1960: On the generation of surface waves by turbulent shear flows. *J. Fluid Mech.*, **7**, 469–478.

Mizuno, S., 1975: Growth of mechanically generated waves under a following wind, I. *Rep. Res. Inst. Appl. Mech. Kyushu Univ.*, **22**, 357–376.

Okuda, K., S. Kawai and Y. Toba, 1977: Measurement of skin friction distribution along the surface of wind waves. *J. Oceanogr. Soc. Japan*, **33**, 190–198.

Okuda, K., 1981: Internal flow structure of short wind waves. Parts I, II and III. Submitted to *J. Oceanogr. Soc. Japan.*

Phillips, O.M. and M.L. Banner, 1974: Wave breaking in the presence of wind drift and swell. *J. Fluid Mech.*, **66**, 625–640.

Toba, Y., 1972: Local balance in the air-sea boundary processes, I. On the growth process of wind waves. *J. Oceanogr. Soc. Japan*, **28**, 109–120.

Toba, Y., 1978: Stochastic form of the growth of wind waves in a single-parameter representation with physical implications. *J. Phys. Oceanogr.*, **8**, 494–507.

Toba, Y., M. Tokuda, K. Okuda and S. Kawai, 1975: Forced convection accompanying wind waves. *J. Oceanogr. Soc. Japan*, **31**, 192–198.

Toba, Y., M. Hatori, Y. Imai and M. Tokuda, 1981: Experimental study on elementary process in wind waves using wind over regular waves. To be published in Proceedings of the IUCRM Symposium on Wave Dynamics and Radio Probing of the Ocean Surface, May 13–20, 1981, Miami Beach.

Tokuda, M. and Y. Toba, 1981: Statistical characteristics of individual waves in laboratory wind waves. I. Individual wave spectra and similarity structure. *J. Oceanogr. Soc. Japan.*, In press.

Yuen, H.C. and B.M. Lake, 1980: Instabilities of waves on deep water. *Ann. Rev. Fluid Mech.*, **12**, 303–334.